

This is a self-archived version of an original article. This version may differ from the original in pagination and typographic details.

Author(s): Välikangas, Juho; Laine, Petteri; Hietaniemi, Marianna; Hu, Tao; Selent, Marcin; Tynjälä, Pekka; Lassi, Ulla

Title: Correlation of aluminum doping and lithiation temperature with electrochemical performance of $\text{LiNi}_{1-x}\text{Al}_x\text{O}_2$ cathode material

Year: 2023

Version: Published version

Copyright: © The Author(s) 2022

Rights: CC BY 4.0

Rights url: <https://creativecommons.org/licenses/by/4.0/>

Please cite the original version:

Välikangas, J., Laine, P., Hietaniemi, M., Hu, T., Selent, M., Tynjälä, P., & Lassi, U. (2023). Correlation of aluminum doping and lithiation temperature with electrochemical performance of $\text{LiNi}_{1-x}\text{Al}_x\text{O}_2$ cathode material. *Journal of Solid State Electrochemistry*, 27(3), 641-654. <https://doi.org/10.1007/s10008-022-05356-y>



Correlation of aluminum doping and lithiation temperature with electrochemical performance of $\text{LiNi}_{1-x}\text{Al}_x\text{O}_2$ cathode material

Juho Välikangas¹ · Petteri Laine¹ · Marianna Hietaniemi¹ · Tao Hu¹ · Marcin Selent³ · Pekka Tynjälä^{1,2} · Ulla Lassi¹

Received: 29 September 2022 / Revised: 5 December 2022 / Accepted: 11 December 2022
© The Author(s) 2022

Abstract

This article presents a process for producing $\text{LiNi}_{1-x}\text{Al}_x\text{O}_2$ ($0 < x < 0.05$) cathode material with high capacity and enhanced cycle properties of 145 mAh/g after 600 cycles. The $\text{LiNi}_{1-x}\text{Al}_x\text{O}_2$ ($0 < x < 0.05$) cathode material is prepared by mixing coprecipitated $\text{Ni}(\text{OH})_2$ with LiOH and $\text{Al}(\text{OH})_3$, followed by lithiation at temperature range of 650–710 °C, after which any residual lithium from lithiation is washed from the particle surfaces. Electrochemical performance was studied within full-cell and half-cell application; in addition, different material characterization methods were carried out to explain structure changes when certain amount of aluminum is introduced in the $\text{LiNi}_{1-x}\text{Al}_x\text{O}_2$ structure. Surface analyses were carried out to demonstrate how washing process changes the chemical environment of the $\text{LiNi}_{1-x}\text{Al}_x\text{O}_2$ secondary particle surface. The results demonstrate how Al doping, lithiation temperature, and the washing process affect the performance of the $\text{LiNi}_{1-x}\text{Al}_x\text{O}_2$ cathode material.

Keywords Lithium-ion battery · LNO · Cathode · Lithium-nickel oxide · Aluminum

Introduction

Lithium-ion batteries based on LiCoO_2 cathode material were first introduced by J. B. Goodenough's group in the 1980s [1], and since then, they have long been the most used cathode material in Li-ion technology, especially portable electronics. Electric vehicle (EV) battery technology relies heavily on cobalt, which is a relatively rare and expensive metal that is a limiting factor for growth of the EV market. There is plenty of ongoing research and development aimed at reducing the amount of cobalt in cathode materials [2]. An attractive candidate for use in cathode materials is LiNiO_2 due to its high theoretical capacity of 272 mAh/g at a reasonable voltage range of 4.2–2.6 V and lower raw material costs than cobalt-based materials. For these reasons, LiNiO_2 has been studied for decades [3–6],

and earlier studies identified several problems with the use of LiNiO_2 as a cathode material, including Li/Ni mixing during synthesis, bad electrochemical cycling stability [4, 7], and thermal instability [8].

Al doping has been studied by a number of researchers. Guilmard et al. [9] prepared 10–50% Al doping during precipitation and demonstrated that it is possible to suppress the phase transition of LiNiO_2 with Al doping. Cao et al. [10] coated $\text{Ni}(\text{OH})_2$ particles with Al species before the lithiation process and showed that 3–7% Al doping improved the performance of LiNiO_2 cathode material. Other studies have recently shown that elements other than Co, such as Al, Mg, and Mn, can stabilize LiNiO_2 structures [11–14].

The present study presents a simple process to produce high-quality $\text{LiNi}_{1-x}\text{Al}_x\text{O}_2$ by adding aluminum during the lithiation process. The results clarify the correlation of the amount of aluminum and lithiation temperature with the properties of $\text{LiNi}_{1-x}\text{Al}_x\text{O}_2$ and show how residual lithium washing after lithiation affects the material's performance. The washing process was conducted to remove LiOH and Li_2CO_3 from the particle surfaces. This washing process is essential for the Ni-based cathode material to avoid forming CO_2 , Co, and H_2 gases during the first charging cycle [15].

✉ Juho Välikangas
juho.valikangas@oulu.fi

¹ Research Unit of Sustainable Chemistry, University of Oulu, P.O. Box 4000, 90014 Oulu, Finland

² University of Jyväskylä, Kokkola University Consortium Chydenius, Talonpojankatu 2B, 67100 Kokkola, Finland

³ Centre for Material Analysis, University of Oulu, P.O. Box 8000, 90014 Oulu, Finland

Experimental

Synthesis of aluminum-modified LiNiO₂

The Ni(OH)₂ precursor precipitated at 50 °C [16] was mixed with LiOH and Al(OH)₃ using Li:Ni:Al molar ratios of 1.04:1–0.95:0–0.05. Samples prepared at 670 °C were later named LNA0%, LNA0.8%, LNA1.2%, LNA1.6%, LNA2.5%, LNA4.1%, and LNA5.2% based on the amount of aluminum in the sample. Excess LiOH was used to compensate for lithium loss during high-temperature calcination and to ensure homogeneous lithiation. The mixtures were calcined with a 2.5 °C/min heating ramp and a 5-h holding time at a temperature of 670 °C in an oxygen atmosphere. Different lithiation temperatures were tested (650 °C, 670 °C, 690 °C, or 710 °C), and samples were named according to their respective quantity of aluminum and calcination temperatures (for example, LNA2.5%690). The material was subsequently milled and sieved to less than 40 µm in dry room conditions.

For the pouch cell tests, the residual lithium and other impurities were washed from the surfaces of the secondary particles with deionized water. The samples were later named according to the quantity of aluminum, lithiation temperature, and W for washed (for example, LNA2.5%690 W). For the LNA4.1% sample, results were obtained for only the unwashed version.

Characterization methods

X-ray diffraction (XRD) was measured with Rigaku SmartLab 9 kW X-ray diffractometers (Rigaku Corporation, Tokyo, Japan) using Co as a source at 40 kV and 135 mA. Diffractograms were collected in the 2θ range (5–120 at 0.01 intervals) with a scan speed of 4.06°/min. Peaks were identified using the database from the International Centre for Diffraction Data (PDF-4 + 2022). A detailed description of the XRD analysis is provided in our earlier paper [16].

Rietveld refinement was carried out with the PDXL ver. 2 suite (Rigaku Corporation) using b-spline background correction and split pseudo-Voigt peak shape modeling against the target phase. The constraints used for modeling were as follows: the same temperature factors for Li1 and Ni1 occupying the 3b site and the same temperature factors for site 3a occupied by Ni2 and Al ions. No vacancies for sites 3a and 3b were allowed (i.e., the total occupancy for each site was 1). Occupancy of oxygen ion was fixed, and its position was set as a free parameter. Occupancy of aluminum was obtained and fixed for the 3a site from ICP measurements of prepared materials, while Ni and Li ions were set as free parameters. Refinement continued

until the parameters converged, and changes in consecutive cycles were below a strict cutoff. In addition, the estimated standard deviation (ESD) was low for the obtained parameters, and the final Rwp was affected by Kb ghost peaks, which did not overlap with observed reflections.

The chemical environment at the surface area (thickness of < 10 nm) was analyzed with X-ray photoelectron spectroscopy (XPS) using a Thermo Fisher Scientific ESCALAB 250Xi XPS system (Thermo Fisher Scientific, Waltham, MA, USA). The powder samples were placed on a gold sample holder, and the high-resolution scan used a pass energy of 20 eV, while the survey scan used a pass energy of 150 eV. The monochromatic Al Kα radiation (1486.7 eV) operated at 20 mA and 15 kV with an X-ray spot size of 900 µm. The Li, Ni, Al, O, and C were measured for all of the samples, and the measurement data were analyzed with Avantage v.5 software (Thermo Fisher Scientific). The charge compensation was carried out by applying the C1s at 284.8 eV as a reference to determine the presented spectra and calibrate the binding energies.

Elemental mapping was obtained with a JEOL JXA-8530F Plus field emission electron probe microanalyzer (EPMA; JEOL, Tokyo, Japan). The epoxy samples were prepared by mixing the epoxy resin and hardener following established procedures and then adding the sample powders at room temperature. The epoxy samples were cured and polished to obtain flat surfaces. The EPMA was equipped with a five-wavelength-dispersive X-ray spectrometer (WDS) and an energy-dispersive X-ray spectroscopy (EDS) detector with a minimum detectable element concentration of 100 ppm.

The microstructures shown in the field-emission scanning electron microscopy (FE-SEM) images were obtained using a Zeiss Sigma FE-SEM (Zeiss Group, Oberkochen, Germany) operating at 5 kV. XRD, EPMA, and FE-SEM were performed at the Centre for Material Analysis of the University of Oulu.

The ICP-OES determinations were carried out with an Agilent 5110 VDV ICP-OES (Agilent Technologies, Santa Clara, CA, USA) equipped with an SPS-4 autosampler, a U-series concentric glass nebulizer, a cyclonic glass double-pass spray chamber, and a 1.8 mm semi-demountable torch. The analysis results are given as the mean value of five replicated measurements. Yttrium (wavelength 371.029) was used as an internal standard to correct for sensitivity drift and matrix effects in the measurements.

Cell assembly and electrochemical characterization

Electrochemical performance testing was carried out using both half-cells with metallic lithium as the counter electrode and full cells with graphite as the anode material. All electrode foils and battery cells were prepared in dry room conditions.

A cathode slurry was prepared with a ThinkyMixer ARE-250 (Thinky Corporation, Tokyo, Japan). The slurry composition was 4% polyvinylidene fluoride (Kureha no. 1100), 4% carbon (Timcal C45) and 92% active material, with 1-methyl-2-pyrrolidinone (Alfa Aesar, anhydrous 99.5%) as a solvent. The slurry was spread on aluminum foil with 100 μm applicators before being dried on a hot plate at 50 °C for 1 h and then placed in a vacuum oven at 120 °C overnight.

The cathode foil was calendered three times before coin cell assembly. The active material loaded on the foil was about 12 mg/cm². Two 2016-type coin cells were assembled from each sample foil, with metallic lithium as the counter electrode and 1 M LiPF₆ in 1:1:1 EC:DEC:DMC as the electrolyte. The cells were cycled 62 times at 25 °C (see Table 1 for the C-rate used). The cells were first charged at a constant current until 4.3 V was reached and then at a constant voltage until the current decreased to 0.015 C for the first two cycles. In subsequent charge cycles, the same method was used, but the current threshold was raised to 0.02 C. Discharge for the first two cycles was performed at a constant current of 0.1 C until 2.6 V was reached and then with a constant voltage until the current decreased to 0.015 C. A subsequent discharge was conducted to 3.0 V with a constant current. The cells were tested at 25 °C. The theoretical capacity used to calculate the C-rate was 200 mAh/g. One electrode pair pouch cell (50 mAh) was prepared with a graphite anode (Hitachi), an electrolyte of 1.15 M LiPF₆ in EC:DMC:EMC (2:4:4), and 1% vinylene carbonate. After the formation cycles, the pouch cells were first charged at a constant current of 0.5 C until 4.2 V was reached and then at a constant voltage until the current decreased to 0.03 C and discharged to 2.5 V at 0.5 C. Every 200 cycles, a capacity check cycle at 0.2 C was run. Before each capacity check, the cells were discharged at 0.2 C [16].

Results and discussion

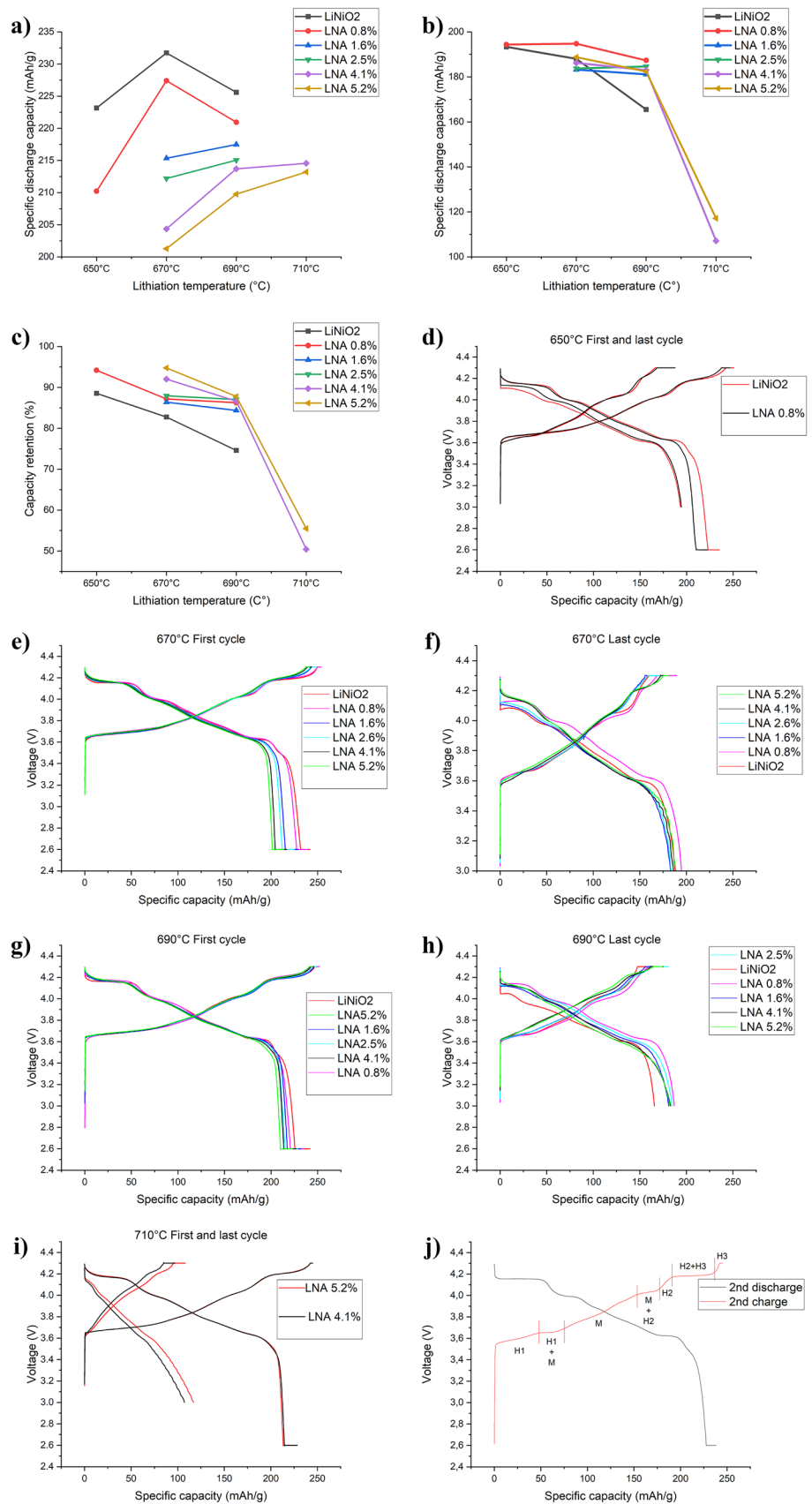
Effect of lithiation temperature and amounts of aluminum on the electrochemical properties of aluminum-modified samples

As shown in our earlier paper, precipitation was performed in a continuous-flow reactor [16]. Here, we studied Al doping (0–5.2 wt%) of LiNiO₂ by optimizing the lithiation temperature for the samples and comparing them with our earlier pure LiNiO₂ results [16]. Figure 1a shows the coin cell test program's first 0.1 °C discharge capacities for the pure LiNiO₂ and aluminum-modified LNA samples. At all three tested temperatures, pure LiNiO₂ had a higher first-cycle discharge capacity than the aluminum-modified samples. For pure LiNiO₂ and

Table 1 Coin cell testing program [16]

Cycle number	1	2	3	4	5	6	7–30	31	32–59	61	62
Charge C-rate	0.1+0.015	0.1+0.015	0.1+0.02	0.1+0.02	0.1+0.02	0.1+0.02	0.2+0.02	0.2+0.02	0.2+0.02	0.2+0.02	0.1+0.02
Discharge C-rate	0.1+0.015	0.1+0.015	0.2	0.33	0.5	1	2	0.2	2	0.2	0.1
Voltage range	4.3–2.6 V	4.3–2.6 V	4.3–3.0 V	4.3–3.0 V	4.3–3.0 V	4.3–3.0 V	4.3–3.0 V	4.3–3.0 V	4.3–3.0 V	4.3–3.0 V	4.3–3.0 V

Fig. 1 **a** First-cycle discharge capacity at a 0.1 °C current for the pure and aluminum-modified LiNiO_2 cathode materials prepared at 650 °C, 670 °C, 690 °C, or 710 °C. **b** The last discharge cycle after a 62-cycle coin cell test program (Table 1) for the pure and aluminum-modified LiNiO_2 cathode materials prepared at 650 °C, 670 °C, 690 °C, or 710 °C. **c** The capacity retention values of the prepared samples after 62 cycles. **d–i** Voltage profiles for the samples prepared at different temperatures. **j** Second cycle charge/discharge voltage profiles for LiNiO_2 lithiated at 670 °C



the LNA0.8% samples, 670 °C had the greatest discharge capacity. Samples with a higher content of aluminum (LNA1.6–LNA5.2%) exhibited a higher capacity for the samples lithiated at 690 °C, compared to results at 670 °C. These results indicate that 1.6–5.2% aluminum modifications to the LiNiO_2 structure using this process required higher lithiation temperatures, such as 690 °C. Figure 1b shows the discharge capacity at 0.1 °C after 62 cycles. The LNA0.8% aluminum-modified sample showed the greatest capacity for all three preparation temperatures, which means that, unlike pure LiNiO_2 , aluminum modification stabilizes the structure during cycling. Figure 1c shows the capacity retention percentage after 62 cycles and reveals that samples with more than 0.8% aluminum had better capacity retention and yielded better results with longer cycle tests. Conversely, capacity retention for LNA4.1% and LNA5.2% lithiated at 710 °C had very poor capacity retention, indicating that 710 °C is a too-high lithiation temperature. Figure 1a shows a low first-cycle capacity for LNA0.8% at 650 °C and a greater capacity for the pure LiNiO_2 , which indicates that aluminum modification hinders the lithiation process for LNA0.8%. The results indicate that aluminum modification of LiNiO_2 during the lithiation process requires temperatures of 670 °C for 0.8–1.6% aluminum and 690 °C for more than 1.6% aluminum for sufficient lithiation when compared with pure LiNiO_2 lithiation. Figure 1 d–i shows the charge and discharge voltage profiles for the samples prepared at different temperatures. For the first cycle voltage, curves were quite similar, and all of the samples showed normal voltage plateaus for LiNiO_2 -type materials. However, after 62 cycles, a clear difference can be seen between the pure and higher aluminum-modified samples. According

to Li et al., pure LiNiO_2 undergoes multiple phase transitions during charge and discharge, including the H1 (first hexagonal) phase to the M (monoclinic) phase, the M phase to the H2 (second hexagonal) phase, and the H2 to H3 (3rd hexagonal) phase [17, 18]. These phase transition can be seen as voltage changes between voltage plateaus in the Fig. 1j voltage profiles. Pure LiNiO_2 crystal lattice suffered an abrupt volume change during the H2 to H3 transition [19], and stabilizing this with Al doping can better explain the cycling properties of Al-doped materials.

Voltage curves showed higher capacity drops at the beginning of the discharge cycle for the pure LiNiO_2 than for the Al-modified samples, and the difference increased with increases in the lithiation temperature, particularly with the last-cycle discharge at 690 °C.

Figure 1h shows the difference between the pure and aluminum-modified samples. The highest aluminum amount in LNA 5.2% shows the lowest voltage drop at 690 °C. This indicates that aluminum modification stabilized the LiNiO_2 crystal structure and enabled better reversibility during high lattice volume changes in the H2 to H3 phase transition, which can be clearly seen in the dQ/dV profiles shown in Fig. 2 a and b. Figure 2b shows that in the last cycle of dQ/dV , pure LiNiO_2 had nearly completely vanished; meanwhile, the aluminum-doped sample showed a clear phase transition.

Effects of washing and amounts of aluminum on $\text{LiNi}_{x-1}\text{Al}_x\text{O}_2$ structures

Table 2 shows the metal ratios of the samples after the washing procedure and before washing for sample

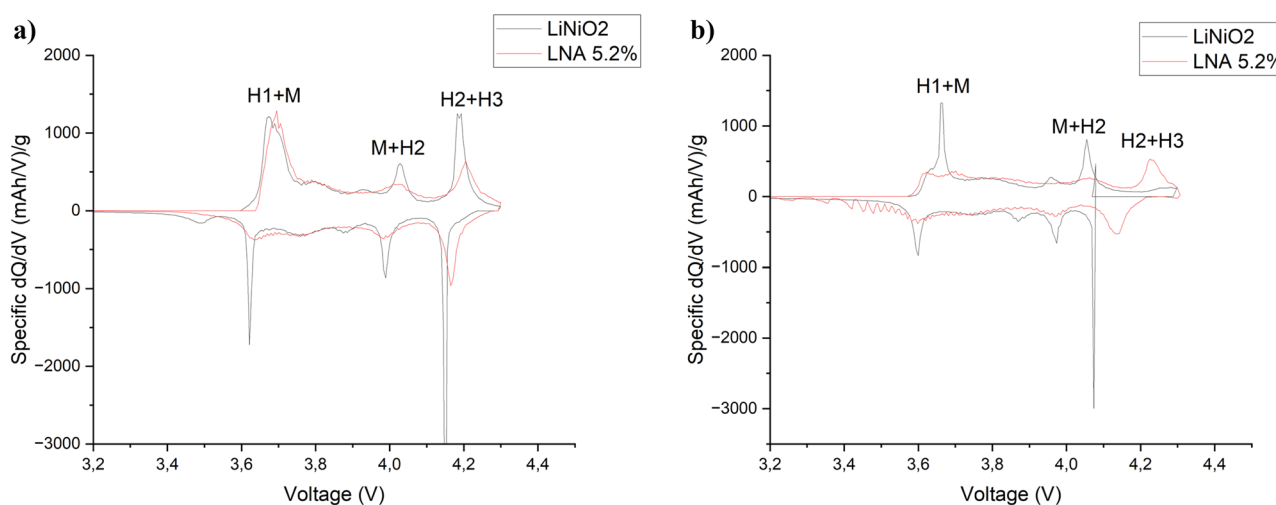


Fig. 2 **a** The first cycle differential capacity profiles (dQ/dV) for pure LiNiO_2 and aluminum-modified LNA 5.2% samples. **b** The last cycle differential capacity profiles (dQ/dV) for pure LiNiO_2 and aluminum-modified LNA 5.2% samples

Table 2 Mole ratios of nickel, cobalt, and aluminum. Impurity content of sulfur and sodium. Lithium and metal (Ni, Al) ratios. All results measured by ICP/OES

Sample	Ni mol %	Co mol %	Al mol %	S mg/g	Na mg/g	Li/Me Ratio
LNA0.8%	99.17	0.01	0.81	2.26	0.18	1.05
LNA0%W	99.98	0.02	0.00	0.13	<0.03	0.99
LNA0.4%W	99.58	0.01	0.41	0.14	<0.03	0.99
LNA0.8%W	99.17	0.02	0.82	0.20	0.02	1.01
LNA1.2%W	98.77	0.01	1.21	0.21	<0.03	1.01
LNA1.6%W	98.35	0.01	1.64	<0.2	0.07	0.99
LNA2.5%W	97.49	0.02	2.50	<0.2	0.08	0.97
LNA5.2%W	94.83	0.00	5.17	<0.3	0.07	0.98

LNA0.8%. All of the samples contained a small amount of cobalt from the nickel sulfate used in the precursor precipitation. Residual lithium and impurities, such as

sulfur and sodium, were effectively removed from the particle surfaces during the washing process. Except for LNA2.5%W and LNA5.2%W, the lithium-to-metal ratios

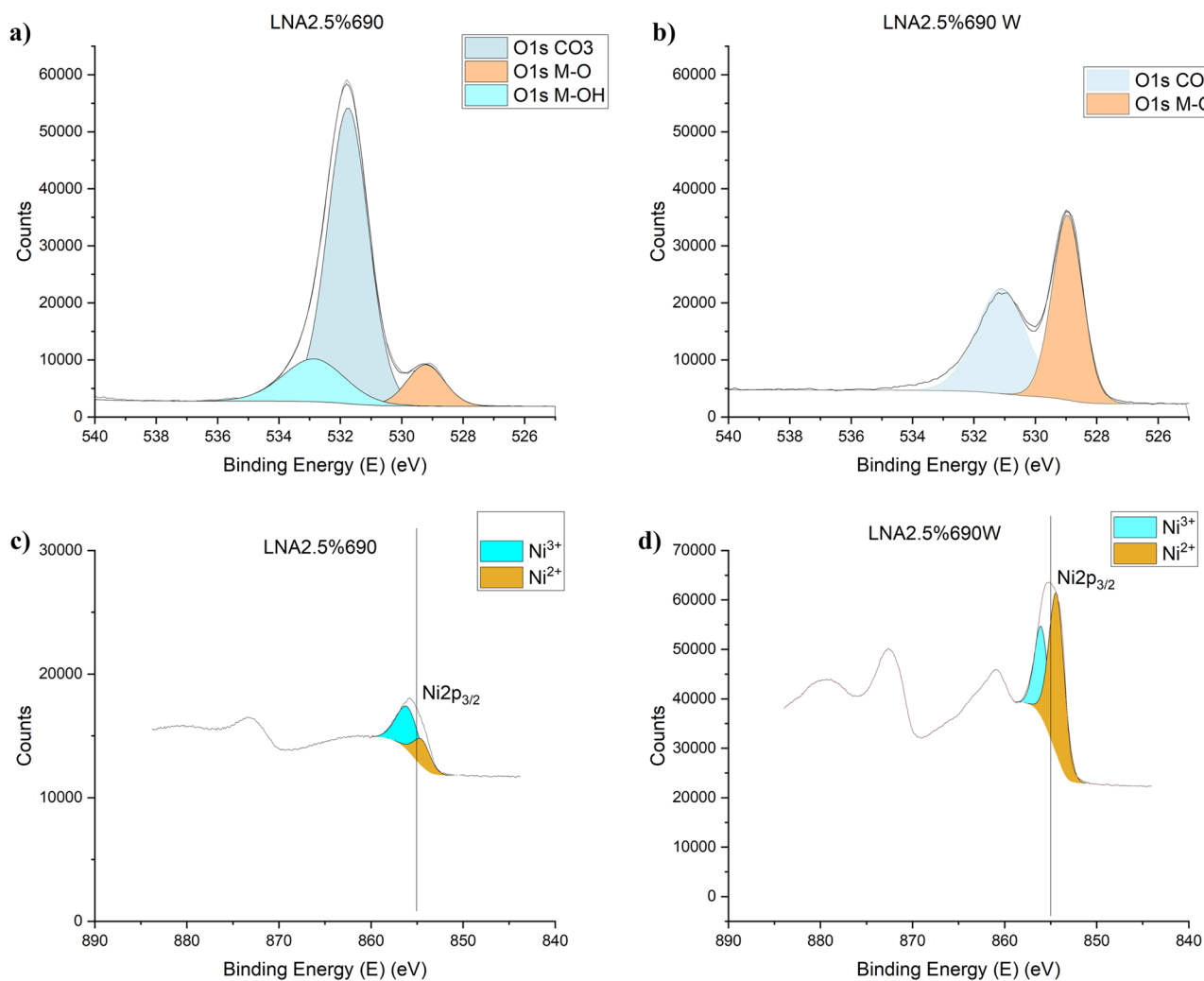


Fig. 3 XPS spectra of **a–b** O1s and **c–d** Ni₂p for unwashed LNA2.5%690 and washed LNA2.5%690 W

were close to 1:1 after washing. The effect of washing on the particle surface compositions and oxidation states was further investigated with XPS analyses. Figure 3a shows the O1 spectra for the sample before washing, with the highest peaks at 531.6 eV assigned to the surface oxygen CO_3 and OH species, indicating the presence of the residual lithium compounds Li_2CO_3 and LiOH . A much lower peak of 529.1 eV was assigned to the lattice oxygen in the metal framework. O1 spectra after washing in Fig. 3b shows that OH species and most of the CO_3 species were washed away, and the amount of lattice oxygen increased in the analyzed area. The Ni2p spectra shown in Fig. 3c and d revealed that before washing, the peak height of $\text{Ni}2\text{P}_{3/2}$ was much lower than after washing because of the high amount of residual lithium species on the surface. The $\text{Ni}2\text{p}_{3/2}$ peak was fitted in the Ni^{2+} (854.4 eV) and Ni^{3+} (856 eV) species, and after washing, the amount of Ni_{2+} increased as compared to Ni_{3+} , indicating a greater amount of delithiated-phase NiO. The effect of NiO on the electrochemical performance is discussed later.

In Fig. 4, the XRD patterns show that the $\text{LiNi}_{1-x}\text{Al}_x\text{O}_2$ materials had an $\alpha\text{-NaFeO}_2$ -type structure (R-3 m), and no impurity phases were detected. Magnification of the XRD pattern peak (003) showed that the peak shifts to smaller angles when the amount of aluminum was increased to 4.1% and 5.2%. A similar peak shift was reported by Liu et al. in their study, when an Ni^{3+} ($r_{\text{Ni}^{3+}} = 0.56 \text{ \AA}$) cation was replaced with smaller Al^{3+} ($r_{\text{Al}^{3+}} = 0.53 \text{ \AA}$) in the NiO_2 slab [20]. Magnification of the peak split 108/110 in the present study showed clear peak splits for all of the samples, indicating a well-ordered layered structure.

Figure 5a shows the lattice parameters obtained from the XRD data. The c -axis increased, and the a -axis slightly decreased as the amount of aluminum increased. The same type of lattice changes were reported by Guilmar et al. and Cao et al. for Al-doped $\text{LiNi}_{1-x}\text{Al}_x\text{O}_2$ materials, and the researchers in both studies concluded that these changes are the results of doping an aluminum element into the NiO_2 slabs [9, 10]. Figure 5a shows that the washing process slightly increased the a - and c -lattice parameters. However, this difference might be due to the residual lithium and impurities being removed from the secondary particle surface [16]. Figure 5b displays the calculated $c/3a$ and 003/004 integrated peak ratios. The $c/3a$ value increased in line with the amount of aluminum in the $\text{LiNi}_{1-x}\text{Al}_x\text{O}_2$ structure, indicating that the amount of aluminum decreases cation/anion mixing in the structure [21]. Furthermore, the Rietveld refinement occupancy data shown in Table 3 confirmed that the amount of Ni^{2+} in the Li^+ 3b site was slightly lower for the aluminum-modified samples (LNA1.6%W and LNA5.2%W). Small differences between the samples are due to optimal lithiation temperatures for the pure LiNiO_2 samples, which already had low levels of cation/anion mixing [9, 10]. A higher level of cation/anion mixing can be observed when the temperature was increased to $710 \text{ }^\circ\text{C}$. In Fig. 4b, it can be seen that the LNA0.8%W sample had the highest value for the integrated peak ratio; however, all the materials showed high integrated peak values, and the differences between the samples are small. Ohzuku et al. showed that electroactive LiNiO_2 has greater integrated intensity ratios of $I(003)/I(104)$ [4]. Figure 5c shows the $c/3a$ ratios and integrated intensity peak ratios for LNA2.5%W and

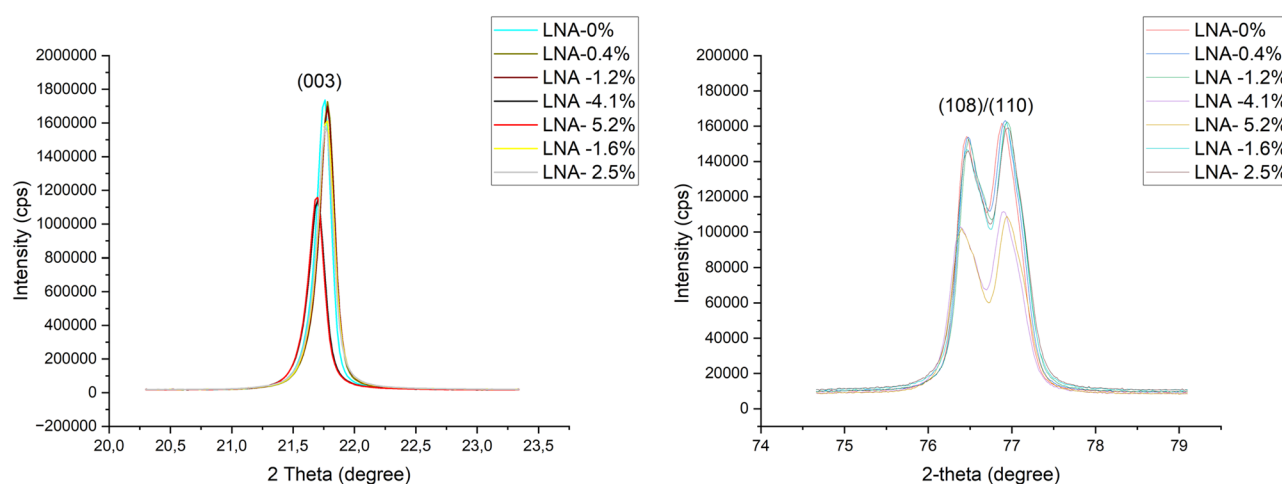


Fig. 4 XRD patterns of different $\text{LiNi}_{1-x}\text{Al}_x\text{O}_2$ materials prepared at $670 \text{ }^\circ\text{C}$ ($x=0, 0.004, 0.008, 0.012, 0.016, 0.025, 0.04, \text{ or } 0.052$); magnifications of peak 003 and peak split (108)/(110)

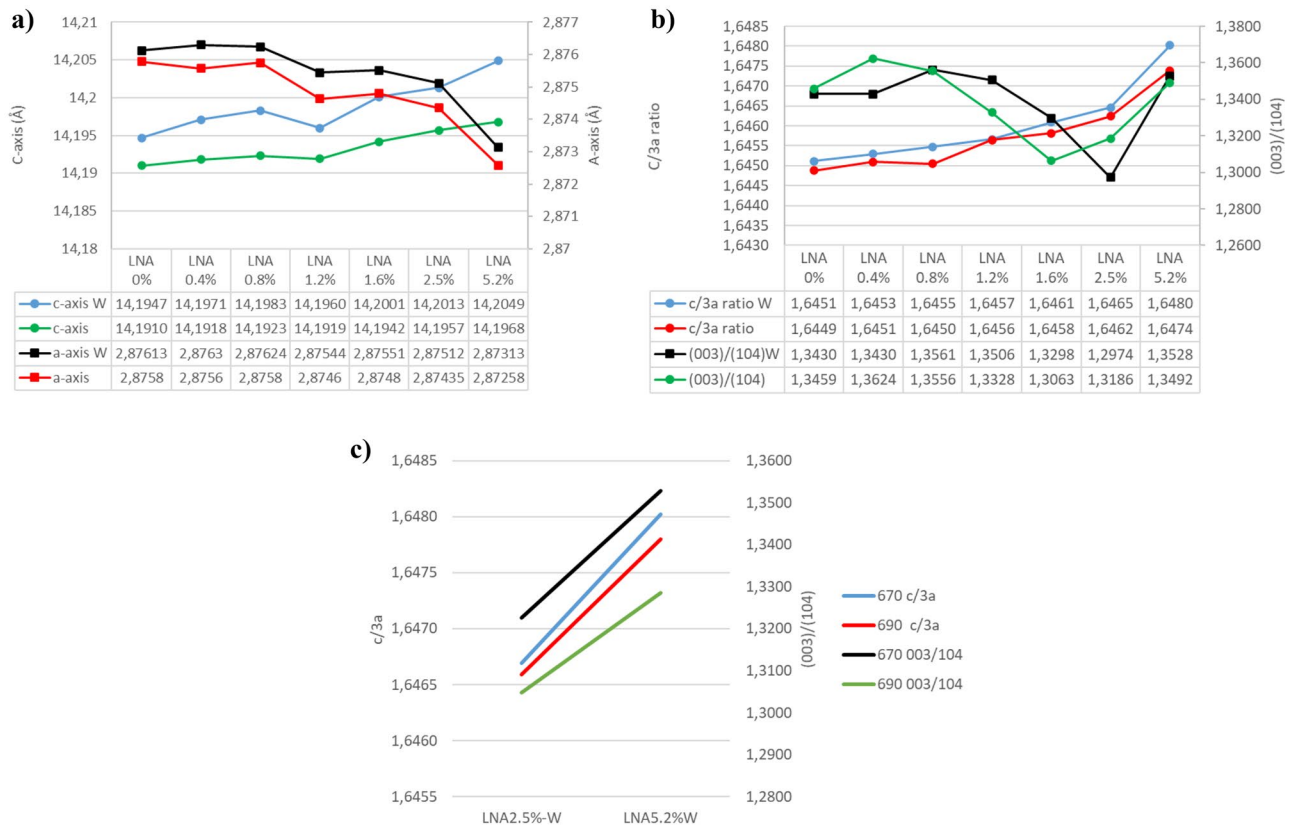


Fig. 5 a Cell parameters and b $C/3a$ ratios and integrated intensity peak ratios for different $\text{LiNi}_{1-x}\text{Al}_x\text{O}_2$ materials prepared at 670 °C. c $C/3a$ ratios and integrated intensity peak ratios for different LNA2.5%W, LNA4.0%W, and LNA5.2% materials prepared at 670 °C or 690 °C

LNA5.2%W prepared at 670 °C and 690 °C. Samples prepared at 670 °C showed the highest integrated intensity peak ratios, and the ratios increased as the aluminum amounts increased in the structures. The $c/3a$ values were slightly higher for samples prepared at 670 °C, which indicates less cation/anion mixing in the structure.

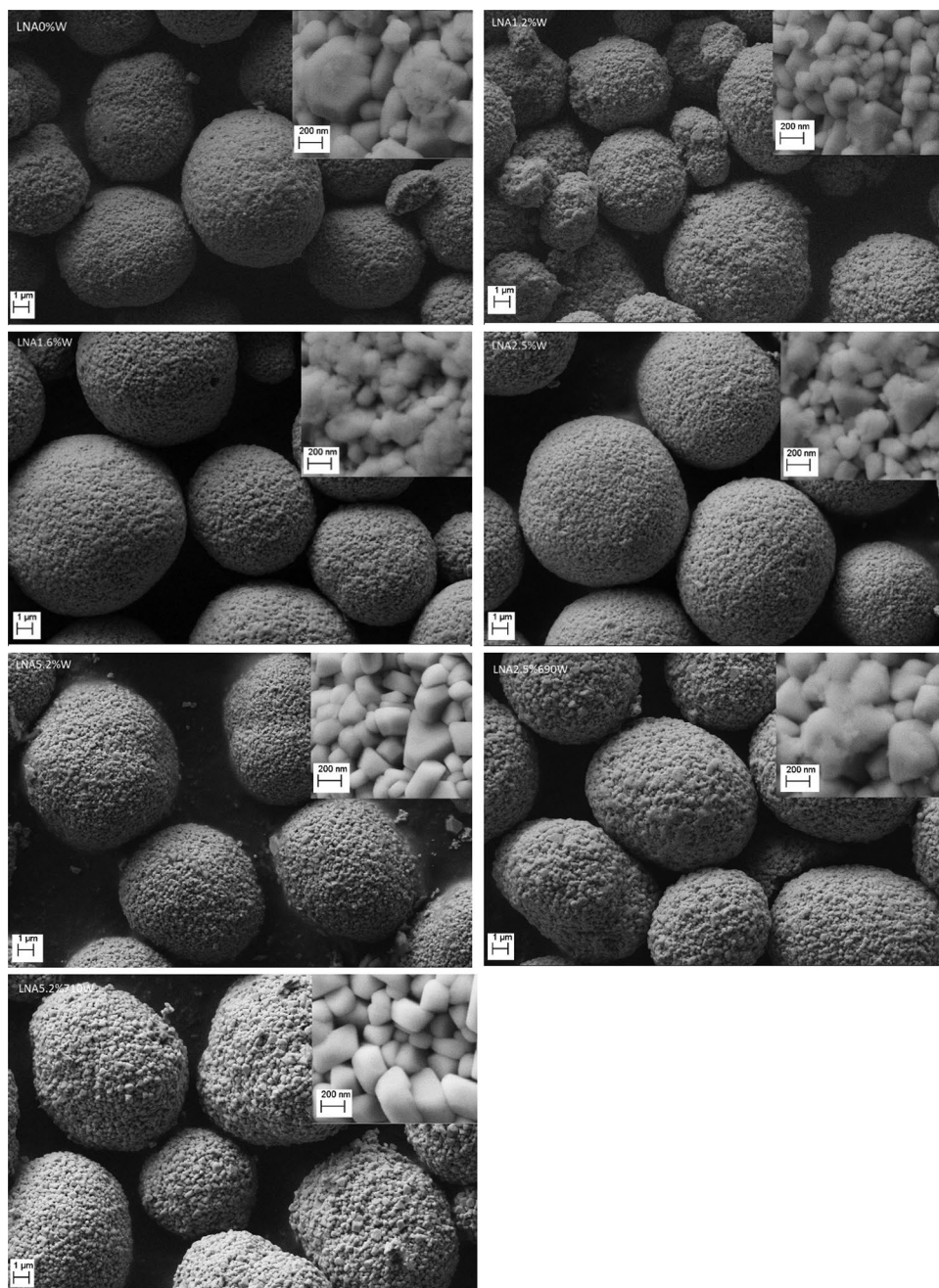
In Fig. 6, the FE-SEM images at 10,000 magnification show that the $\text{LiNi}_{1-x}\text{Al}_x\text{O}_2$ secondary particles retained their round-shaped morphology through the mixing, lithiation, washing, and sieving processes. The images at 75,000

magnification show the secondary particle surfaces, and that the primary particles have a similar shape and size of about 200 nm for the samples prepared at 670 °C. Samples prepared at 690 °C and 710 °C showed slightly larger primary particles compared to samples prepared at 670 °C. EPMA/WDS was performed on the cross sections of the samples to obtain more information about aluminum distribution, with the results illustrated in Fig. 7. Elemental mapping showed that aluminum was uniformly distributed, and the aluminum element contents increased in the Al-doping ratio of the samples.

Table 3 Lattice occupancies of the Li, Ni, and Al sites

Sample	Occupancy					Rwp (%)
	Li1 (3b)	Ni1 (3b)	Ni2 (3a)	Al1 (3a)	O1 (6c)	
LNA0%W	0.9798	0.0202	1.0000	0.0000	1.0000	6.37%
LNA1.6%W	0.9800	0.0200	0.9879	0.0121	1.0000	6.09%
LNA5.2%W	0.9804	0.0196	0.9478	0.0522	1.0000	5.35%
LNA5.2%690 W	0.9800	0.0200	0.9417	0.0583	1.0000	5.90%
LNA5.2%710 W	0.9771	0.0229	0.9486	0.0514	1.0000	5.75%

Fig. 6 FE-SEM images of LNA0%W, LNA1.2%W, LNA1.6%W, LNA2.5%W, and LNA5.2%W samples prepared at 670 °C. Samples LNA2.5%690 W and LNA5.2%710 W prepared at different temperatures, shown at magnifications of 10,000 and 75,000



Electrochemical performance of $\text{LiNi}_{x-1}\text{Al}_x\text{O}_2$ cathode materials

Table 4 shows the first-cycle charge capacities, discharge capacities, and capacity retention after 62 cycles for the unwashed samples, and Table 5 displays the data for the washed samples. Before washing, the first-cycle

capacity started to decrease when the amount of aluminum increased to 1.2%. Lower amounts of aluminum did not affect the first-cycle capacities. When aluminum modification exceeded 1.2%, capacity linearly decreased. For the samples prepared at 670 °C, first-cycle efficiency decreased, and capacity retention increased when the amount of aluminum increased. For the samples

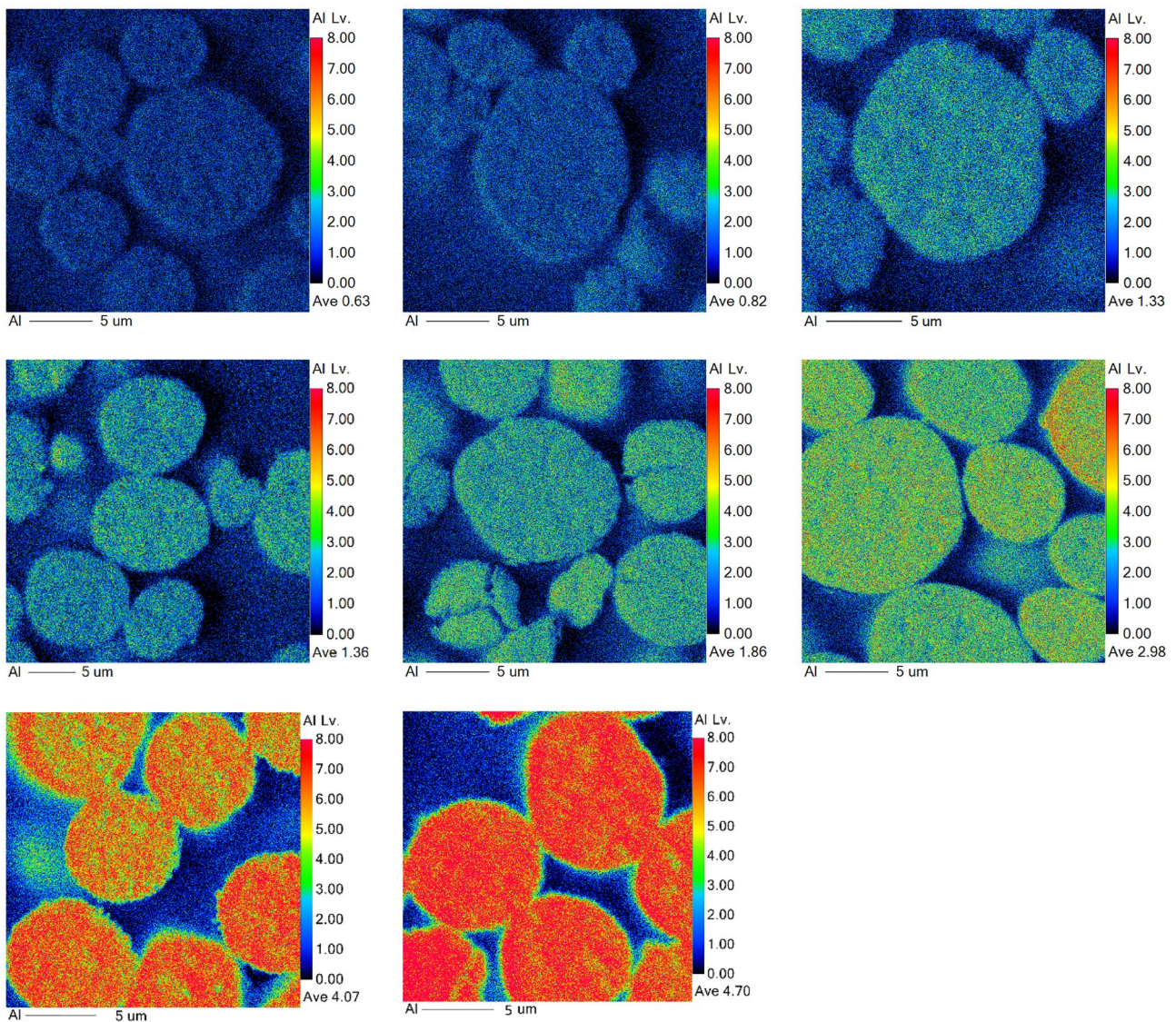


Fig. 7 Elemental mapping of aluminum for LNA0%670 W, LNA0.4%670 W, LNA0.8%670 W, LNA1.2%670 W, LNA 1.6%670 W, LNA2.5%670 W, LNA4.1%670 W, and LNA5.2%670 W with EPMA

LNA1.6–LNA5.2%, increasing the lithiation temperature to 690 °C resulted in increased first-cycle capacities and decreased capacity retention after 62 cycles. Table 5 shows that after the residual lithium was washed from the particle surfaces, the first-cycle capacities decreased as compared to the unwashed samples. However, aluminum modification seemed to inhibit unwanted reactions on the particle surfaces during the washing process. In particular, the LNA1.2%670 W sample showed only a 6.8 mAh/g decrease in the first-cycle capacity compared to

the unwashed LNA1.2% sample. The LNA1.2%W had the highest discharge capacity of 175.8 mAh/g after 62 cycles.

Figure 8a, b show the voltage curves and cycling performances of unwashed LNA0%670, LNA1.2%, and washed LNA0%W, LNA1.2%W samples. The washed samples had higher charge voltages and lower discharge voltages, which indicates higher resistance, and that the washing process lowered ionic conductivity on the secondary particle surfaces. This was confirmed as a larger anodic and cathodic peak separation for the washed

Table 4 First-cycle performance and capacity retention after 62 cycles for samples LNA1.6%–LNA5.2% prepared at 670 °C and at 690 °C

Sample	Charge 4.3 V 0.1C + 0.015C (1st)	DC 3.0 V 0.1C (1st)	DC 2.6 V 0.1C (1st)	0.1C eff. 2.6v (1st)	DC 3.0 V 0.1C (62)	Retention after 62 cycles
	mAh/g	mAh/g	mAh/g	%	mAh/g	%
LNA0%	251.6	221.1	224.9	89.4	193.6	87.6
LNA0.4%	250.9	220.1	224.0	89.3	194.9	88.5
LNA0.8%	251.4	220.4	223.7	89.0	196.8	89.3
LNA1.2%	248.5	215.8	219.9	88.5	195.9	90.8
LNA1.6%	248.6	212.1	215.3	86.6	183.3	86.4
LNA2.5%	248.8	208.9	212.2	85.3	183.7	87.9
LNA4.1%	243.9	202.4	204.4	83.8	186.2	92.0
LNA5.2%	241.2	199.2	201.3	83.4	188.8	94.7
LNA1.6%690	249.1	214.7	217.5	87.3	181.1	84.4
LNA2.5%690	247.6	212.1	215.0	86.9	184.6	87.1
LNA4.1%690	245.7	211.2	213.7	87.0	183.0	86.6
LNA5.2%690	244.4	207.8	209.8	85.8	182.4	87.8

sample in the dQ/dV profiles shown in Fig. 8c–f. Furthermore, XPS analyses shown in Fig. 3 revealed that the amount of Ni²⁺ increased in the washed sample, indicating the presence of NiO octahedra on the secondary particle surface. Xiong et al. showed a similar effect for LiNi_{0.8}Mn_{0.1}Co_{0.1}O₂ material after washing and concluded that washing can lead to chemical delithiation accompanied by the loss of oxygen from the crystal lattice. Defective NiO octahedra cannot move electrons as well as a pristine surface, and the amount of Li⁺ is reduced from the system, which explains lower rates of performance and lower specific capacities of the washed material [22]. Figure 9a shows how different levels of aluminum modifications and the washing process affected the cyclability properties in full-cell applications for the samples prepared at 670 °C. The unwashed LNA0.8% sample showed the highest discharge capacity at 209.3

mAh/g at the beginning of the test, but the capacity decreased much faster during cycling compared to the washed LNA0.8%W sample. LNA1.2%W showed the highest initial capacity among the washed Al-doped samples prepared at 670 °C. The capacity for the first-check cycle was at 189.5 mAh/g, and it was at 140.3 mAh/g after 600 cycles. LNA1.6% showed a slightly higher capacity of 142.7 after 600 cycles. The LNA5.2%W sample showed low initial capacity; however, its cycling stability was better than that of other samples.

Figure 9b displays the full-cell results for the samples prepared at 690 °C or 710 °C and for LNA1.6%W prepared at 670 °C. After 600 cycles, LNA2.5% prepared at 690 °C had the highest discharge capacity of 145.2 mAh/g. Higher and lower temperatures, with different amounts of aluminum, resulted in slightly lower capacities.

Table 5 First-cycle performance and capacity retention after 62 cycles for the washed samples prepared at 670 °C

Sample	Charge 4.3 V 0.1C + 0.015C (1st)	DC 3.0 V 0.1C (1st)	DC 2.6 V 0.1C (1st)	0.1C eff. 2.6v (1st)	DC 3.0 V 0.1C (62)	Retention after 62 cycles
	mAh/g	mAh/g	mAh/g	%	mAh/g	%
LNA0%W	239.7	203.2	207.1	86.4	163.5	80.5
LNA0.4%W	236.9	200.3	204.3	86.2	160.1	79.9
LNA0.8%W	238.2	202.7	206.4	86.6	164.1	81.0
LNA1.2%W	243.9	209.0	212.2	87.0	175.8	84.1
LNA1.6%W	236.7	201.2	205.7	86.9	171.7	85.3
LNA2.5%W	233.3	198.5	203.0	87.0	169.4	85.3
LNA5.2%W	224.2	190.3	194.4	86.7	165.2	86.8

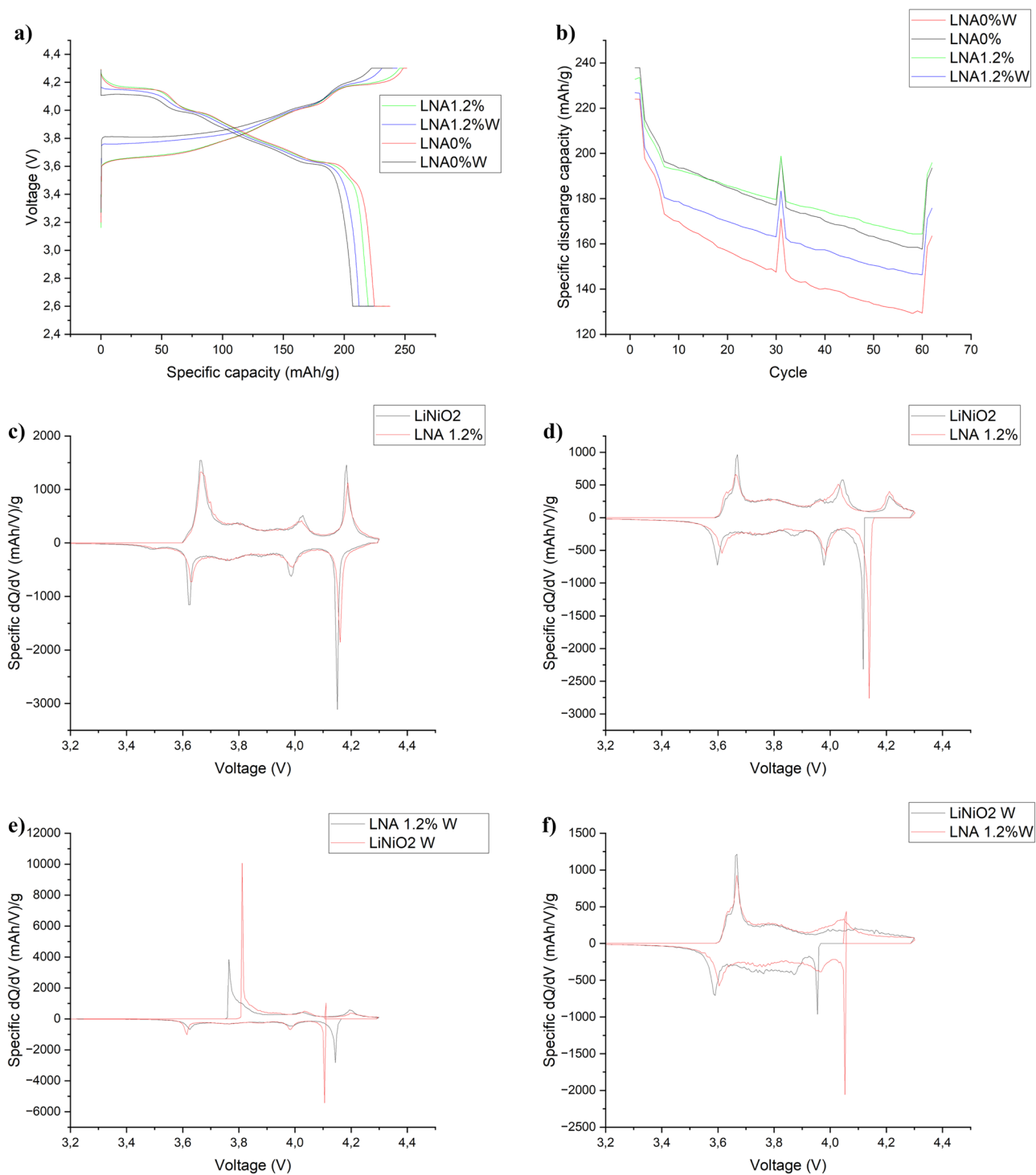


Fig. 8 **a** Initial charge and discharge curves of LNA0% and LNA1.2% before and after washing. **b** Half-cell cycling performance before and after washing. **c** First-cycle dQ/dV of LiNiO₂ and LNA1.2%. **d**

Last-cycle dQ/dV of LiNiO₂ and LNA1.2%. **e** First-cycle dQ/dV of washed LiNiO₂W and LNA1.2%W. **f** Last-cycle dQ/dV of washed LiNiO₂W and LNA1.2%W

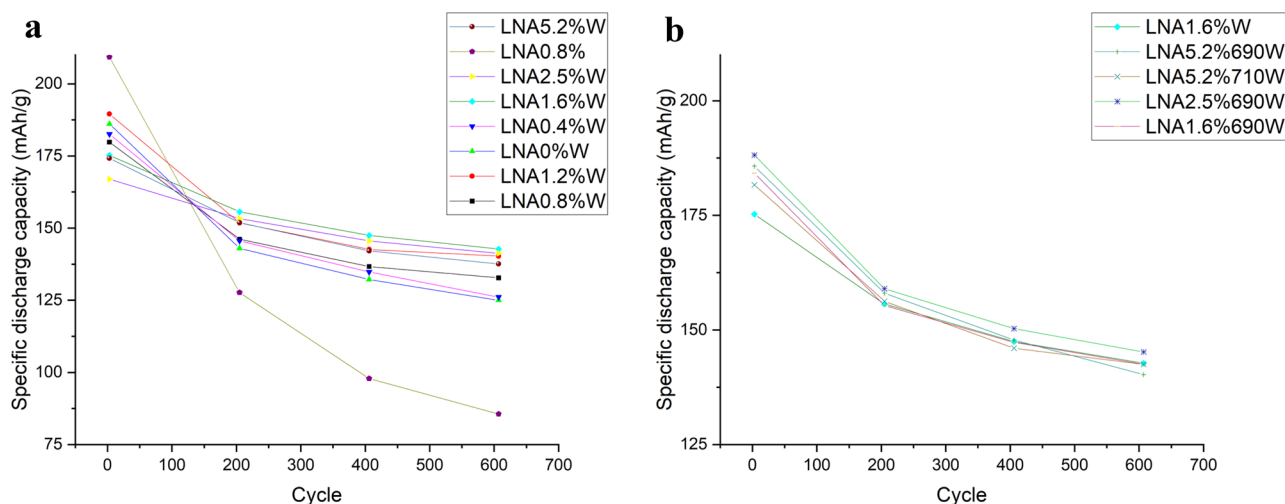


Fig. 9 Specific discharge capacity of 0.2 °C capacity check cycles between 0.5 °C cycling tests in the voltage range of 4.2–2.8 V for the samples prepared at **a** 670 °C and **b** at the different temperatures of

LNA1.6%W at 670 °C; LNA2.5%W, LNA5%W, and LNA1.6%W at 690 °C; and LNA5.2%W at 710 °C

Conclusions

Different amounts of aluminum were added to the $\text{LiNi}_{1-x}\text{Al}_x\text{O}_2$ structure during the lithiation process with a temperature range of 650–710 °C. The results showed that when increasing the amount of aluminum, the lithiation temperature should also be increased. At a lithiation temperature of 670 °C, the best results of 142.7 mAh/g after 600 cycles were achieved with 1.6% aluminum, whereas at 690 °C, the best results of 145.2 mAh/g after 600 cycles were achieved with 2.5% aluminum. Greater amounts of aluminum and higher lithiation temperatures did not result in better electrochemical performance in long-term cycling tests. Enhanced cycle properties of aluminum-modified samples can be explained by more stable crystal structure and better reversibility especially during high lattice volume changes in the H2 to H3 phase transition.

The washing process after lithiation effectively removed residual lithium and impurities from the material surfaces. However, it also lowered the conductivity of the material surface and decreased electrochemical performance. Future research will focus on preventing the unwanted effects of the washing process on the $\text{LiNi}_{1-x}\text{Al}_x\text{O}_2$ surface structure.

Acknowledgements The authors wish to thank Mr. Jaakko Pulkkinen and Ms. Jessica Nuorala for the help with the processing of the samples.

Author contribution Conceptualization, JV, PL, PT, MH, TH, and UL; methodology, JV, PL, PT, MH, and TH; validation, JV, PL, PT, MH, and TH; formal analysis, JV, TH, and MS; investigation, JV and TH; resources, JV, PL, TH, MH, and PT; data curation, JV, PL, PT, MH,

and TH; writing—original draft preparation, JV, PL, PT, MH, MS, TH, and UL; writing—review and editing, JV, PL, PT, MH, TH, and UL; visualization, JV, PL, PT, MH, TH, and UL; supervision, UL; project administration, UL; and funding acquisition, UL. All authors have read and agreed to the published version of the manuscript.

Funding Open Access funding provided by University of Oulu including Oulu University Hospital. The authors acknowledge Business Finland for research funding 2021–2024 (University of Oulu, BATCircle2.0, No. 44612/31/2020)

Declarations

Conflict of interest The authors declare no competing interests.

Open Access This article is licensed under a Creative Commons Attribution 4.0 International License, which permits use, sharing, adaptation, distribution and reproduction in any medium or format, as long as you give appropriate credit to the original author(s) and the source, provide a link to the Creative Commons licence, and indicate if changes were made. The images or other third party material in this article are included in the article's Creative Commons licence, unless indicated otherwise in a credit line to the material. If material is not included in the article's Creative Commons licence and your intended use is not permitted by statutory regulation or exceeds the permitted use, you will need to obtain permission directly from the copyright holder. To view a copy of this licence, visit <http://creativecommons.org/licenses/by/4.0/>.

References

- Mizushima K, Jones PC, Wiseman PJ, Goodenough JB (1980) Li_xCoO_2 ($0 < x < 1$): a new cathode material for batteries of high energy density. *Mater Res Bull* 15:783–789. [https://doi.org/10.1016/0025-5408\(80\)90012-4](https://doi.org/10.1016/0025-5408(80)90012-4)
- Kim Y, Seong WM, Manthiram A (2021) Cobalt-free, high-nickel layered oxide cathodes for lithium-ion batteries: progress,

- challenges, and perspectives. *Energy Storage Mater* 34:250–259. <https://doi.org/10.1016/j.ensm.2020.09.020>
- Arai H (1995) Characterization and cathode performance of $\text{Li}_{1-x}\text{Ni}_x + x\text{O}_2$ prepared with the excess lithium method. *Solid State Ion* 80:261–269. [https://doi.org/10.1016/0167-2738\(95\)00144-U](https://doi.org/10.1016/0167-2738(95)00144-U)
 - Ohzuku T, Ueda A, Nagayama M (1993) Electrochemistry and structural chemistry of LiNiO_2 (R3m) for 4 volt secondary lithium cells. *J Electrochem Soc* 140:1862–1870. <https://doi.org/10.1149/1.2220730>
 - Megahed S, Ebner W (1995) Lithium-ion battery for electronic applications. *J Power Sources* 54:155–162. [https://doi.org/10.1016/0378-7753\(94\)02059-C](https://doi.org/10.1016/0378-7753(94)02059-C)
 - Bianchini M, Roca-Ayats M, Hartmann P et al (2019) There and back again—the journey of LiNiO_2 as a cathode active material. *Angewandte Chemie (International ed)* 58:10434–10458. <https://doi.org/10.1002/anie.201812472>
 - Delmas C, Ménétrier M, Croguennec L et al (1999) An overview of the $\text{Li}(\text{Ni}, \text{M})\text{O}_2$ systems: syntheses, structures and properties. *Electrochim Acta* 45:243–253. [https://doi.org/10.1016/S0013-4686\(99\)00208-X](https://doi.org/10.1016/S0013-4686(99)00208-X)
 - Cormier MME, Zhang N, Liu A et al (2019) Impact of dopants (Al, Mg, Mn, Co) on the reactivity of Li_xNiO_2 with the electrolyte of Li-ion batteries. *J Electrochem Soc* 166:A2826–A2833. <https://doi.org/10.1149/2.0491913jes>
 - Guilmard M, Rougier A, Grüne M et al (2003) Effects of aluminum on the structural and electrochemical properties of LiNiO_2 . *J Power Sources* 115:305–314. [https://doi.org/10.1016/S0378-7753\(03\)00012-0](https://doi.org/10.1016/S0378-7753(03)00012-0)
 - Cao H, Du F, Adkins J et al (2020) Al-doping induced superior lithium ion storage capability of LiNiO_2 spheres. *Ceram Int* 46:20050–20060. <https://doi.org/10.1016/j.ceramint.2020.05.078>
 - Li H, Cormier M, Zhang N et al (2019) Is cobalt needed in Ni-rich positive electrode materials for lithium ion batteries? *J Electrochem Soc* 166:A429–A439. <https://doi.org/10.1149/2.1381902jes>
 - Mu L, Kan WH, Kuai C et al (2020) Structural and electrochemical impacts of Mg/Mn dual dopants on the LiNiO_2 cathode in Li-metal batteries. *ACS Appl Mater Interfaces* 12:12874–12882. <https://doi.org/10.1021/acsami.0c00111>
 - Li W, Lee S, Manthiram A (2020) High-nickel NMA: a cobalt-free alternative to NMC and NCA cathodes for lithium-ion batteries. *Advanced materials (Weinheim)* 32:2002718–n/a. <https://doi.org/10.1002/adma.202002718>
 - Mu L, Zhang R, Kan WH et al (2019) Dopant distribution in Co-free high-energy layered cathode materials. *Chem Mater* 31:9769–9776. <https://doi.org/10.1021/acs.chemmater.9b03603>
 - Kim J, Hong Y, Ryu KS et al (2006) Washing effect of a $\text{LiNi}_0.83\text{Co}_0.15\text{Al}_0.02\text{O}_2$ cathode in water. *Electrochem Solid-State Lett* 9. <https://doi.org/10.1149/1.2135427>
 - Välikangas J, Laine P, Hietaniemi M et al (2020) Precipitation and calcination of high-capacity LiNiO_2 cathode material for lithium-ion batteries. *Appl Sci* 10:8988. <https://doi.org/10.3390/app10248988>
 - Li H, Zhang N, Li J, Dahn JR (2018) Updating the structure and electrochemistry of Li_xNiO_2 for $0 \leq x \leq 1$. *J Electrochem Soc* 165:A2985–A2993. <https://doi.org/10.1149/2.0381813jes>
 - Li W, Reimers JN, Dahn JR (1993) In situ x-ray diffraction and electrochemical studies of $\text{Li}_{1-x}\text{NiO}_2$. *Solid State Ion* 67. [https://doi.org/10.1016/0167-2738\(93\)90317-V](https://doi.org/10.1016/0167-2738(93)90317-V)
 - Ryu H-H, Park K-J, Yoon CS, Sun Y-K (2018) Capacity fading of Ni-rich $\text{Li}[\text{Ni}_x\text{Co}_y\text{Mn}_{1-x-y}]\text{O}_2$ ($0.6 \leq x \leq 0.95$) cathodes for high-energy-density lithium-ion batteries: bulk or surface degradation? *Chem Mater* 30:1155–1163. <https://doi.org/10.1021/acs.chemmater.7b05269>
 - Liu Z, Zhen H, Kim Y, Liang C (2011) Synthesis of LiNiO_2 cathode materials with homogeneous Al doping at the atomic level. *J Power Sources* 196. <https://doi.org/10.1016/j.jpowsour.2011.08.059>
 - Whittingham MS (2004) Lithium batteries and cathode materials. *Chem Rev* 104:4271–4302. <https://doi.org/10.1021/cr020731c>
 - Xiong X, Wang Z, Yue P et al (2013) Washing effects on electrochemical performance and storage characteristics of $\text{LiNi}_0.8\text{Co}_0.1\text{Mn}_0.1\text{O}_2$ as cathode material for lithium-ion batteries. *J Power Sources* 222:318–325. <https://doi.org/10.1016/j.jpowsour.2012.08.029>

Publisher's Note Springer Nature remains neutral with regard to jurisdictional claims in published maps and institutional affiliations.